A molecular state of correlated electrons in a quantum dot

SOKRATIS KALLIAKOS[1], MASSIMO RONTANI[2]*, VITTORIO PELLEGRINI[1]*, CÉSAR PASCUAL GARCÍA[1], ARON PINCZUK[3,4], GUIDO GOLDONI[2], ELISA MOLINARI[2], LOREN N. PFEIFFER[4] AND KEN W. WEST[4]

[1]NEST INFM-CNR and Scuola Normale Superiore, 56126 Pisa, Italy
[2]S3 INFM-CNR and Department of Physics, University of Modena and Reggio Emilia, 41100 Modena, Italy
[3]Depts of Appl. Phys and Appl. Math. and of Physics, Columbia University, New York 10027, USA
[4]Bell Laboratories, Alcatel-Lucent, Murray Hill, New Jersey 07974, USA
*e-mail: rontani@unimore.it; vp@sns.it

Published online: 20 April 2008; doi:10.1038/nphys944

Correlation among particles in finite quantum systems leads to complex behaviour and novel states of matter. One remarkable example is predicted to occur in a semiconductor quantum dot[1–3], where at vanishing electron density the Coulomb interaction between electrons rigidly fixes their relative positions as those of the nuclei in a molecule[4–14]. In this limit, the neutral few-body excitations are roto-vibrations, which have either rigid-rotor or relative-motion character[15]. In the weak correlation regime, on the contrary, the Coriolis force mixes rotational and vibrational motions. Here, we report evidence for roto-vibrational modes of an electron molecular state at densities for which electron localization is not yet fully achieved. We probe these collective modes by using inelastic light scattering[16–18] in quantum dots containing four electrons[19]. Spectra of low-lying excitations associated with changes of the relative-motion wavefunction—the analogues of the vibration modes of a conventional molecule—do not depend on the rotational state represented by the total angular momentum. Theoretical simulations by the configuration-interaction method[20] are in agreement with the observed roto-vibrational modes and indicate that such molecular excitations develop at the onset of short-range correlation.

Whereas vibrations in ordinary molecules consist of oscillations of the heavy nuclei around their equilibrium positions, electrons in quantum dots, such as those in Fig. 1, are described by a probability distribution function. In the absence of disorder, electrons become fully localized only in the limiting case of vanishing density where they form a rigid rotor. In the opposite non-interacting limit, the uncorrelated quantum-dot electrons experience significant Coriolis forces in the rotational states. We expect that at finite density, when the quantum-mechanical correlations are sufficiently strong[21], the relative motion gets decoupled from the rigid rotation of the system, yielding a sequence of molecular-like energy levels labelled by the vibrational (v) and angular momentum (M) quantum numbers, respectively, as shown in Fig. 2b. The insensitivity of the energy of the vibrational modes to the value of M thus provides the signature of the emergence of this correlated state in quantum dots at experimentally accessible density regimes.

To probe these molecular-like roto-vibrational modes of correlated electrons in quantum dots, we have developed the experimental set-up for inelastic light scattering as shown in Fig. 1a. To improve the signal above the noise level, the experiments were carried out in an array composed of 10^4 nominally identical modulation-doped GaAs/AlGaAs quantum dots realized by nanolithography and dry etching. The homogeneity achieved in both lateral size and number of confined electrons of each quantum dot of the array was demonstrated by microphotoluminescence[22]. These nanostructures have an effective lateral size much smaller than their geometrical diameter D, owing to the large depletion width of $\approx$90 nm at the electron densities of $n = 1.1 \times 10^{11}$ cm^{-2} of the modulation-doped quantum well used here[19,23]. In addition, the in-plane confinement potential can be well approximated by a parabola with typical confinement energies in the range $\hbar\omega_0 = 1$–4 meV (ref. 19). This leads to a Fock–Darwin shell structure for non-interacting electrons[1], which has been observed by both transport[24] and inelastic light scattering experiments[16–18], and to the appearance of a Kohn mode in the far-infrared spectra[25].

In our experiment on quantum dots with four electrons (see the Methods section), the rotational state with angular momentum M is tuned by application of a magnetic field[26,27]. In fact, according to Hund's rule, the four-electron ground state at $B = 0$ T is a spin triplet with zero total angular momentum, $(S, M) = (1, 0)$. The excitation spectrum in the spin channel (shown in the bottom part of Fig. 2a) is therefore characterized by the intershell monopole spin excitation (peak S_B) (ref. 19), corresponding to $\Delta S = -1$ and $\Delta M = 0$, from the $B = 0$ triplet ground state to a singlet excited state $(1, 0) \rightarrow (0, 0)$. The application of a moderate magnetic field, B, perpendicular to the quantum-dot plane, induces a ground-state transition to a singlet state with $M = 2$, $(S, M) = (0, 2)$ (ref. 24). This transition, expected when the cyclotron energy approximately equals the exchange term[24] (below $B \approx 0.5$ T for typical densities), appears in the collective spin spectra as a change of the signal at energies close to the S_B peak (shaded area in Fig. 2a). The increased scattering intensity at 0.2–0.3 T (Fig. 2a, inset) is due to the emergence, around 5.5 meV, of three closely spaced spin excitations of the new ground state (0,2) as predicted by the configuration-interaction calculations (arrows in the middle panel of Fig. 2a, see the Methods section). The energy positions of all spin excitations are well reproduced by our model with $\hbar\omega_0 = 3.75$ meV, corresponding to the dimensionless density parameter (Coulomb-to-kinetic energy ratio) $r_S = 1.71$, where $r_S = 1/[a_B^*(\pi \cdot n)^{1/2}]$, a_B^* is the effective

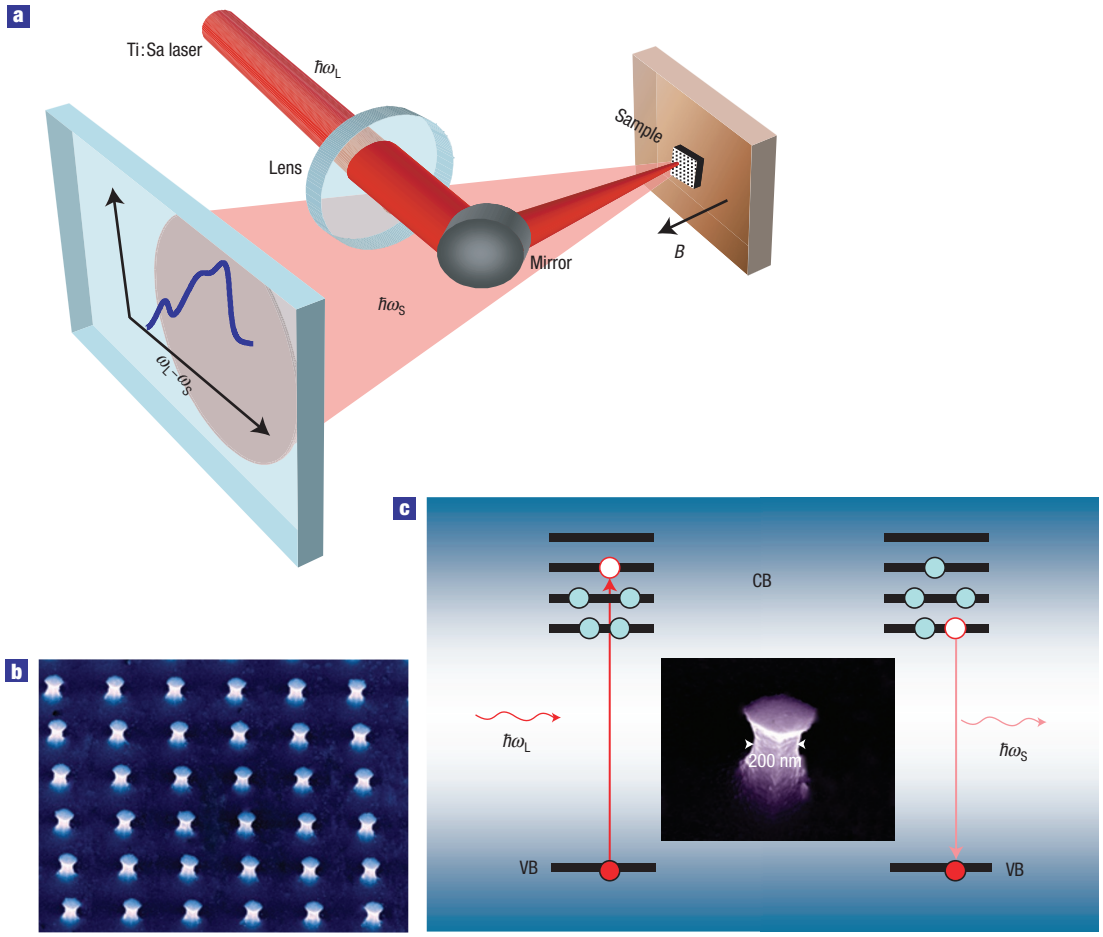

Figure 1 Resonant inelastic light scattering. a, The inelastic light scattering set-up in the backscattering geometry (see the Methods section). **b**, SEM image of an array of quantum dots. **c**, A scheme of the experiment. An incident photon at $\hbar\omega_L$ resonating with a transition close to the gap between conduction (CB) and valence (VB) bands is absorbed creating an electron–hole pair and a scattered photon at $\hbar\omega_S$ is emitted with annihilation of a different electron–hole pair, leaving an excitation of energy $\hbar\omega_L - \hbar\omega_S$. The electronic configurations shown are the main configuration-interaction contributions to the S_C transition. Inset: SEM image of a single quantum dot.

Bohr radius, and the density n is estimated as in ref. 19. The ground-state spin transition is also in excellent agreement with the configuration-interaction prediction of the transition taking place at $B = 0.276$ T (Fig. 2a, inset). We remark that B is too small here to enforce localization[26–28].

Signatures of formation of the roto-vibrational excitations of the correlated electron state, which are captured by the schematic energy level sequence shown in Fig. 2b, can be sought by comparing the excitations of the two ground states with $M = 0$ and $M = 2$, respectively. We focus on the low-lying spin and charge modes shown in Fig. 3 (left: experimental data; right: configuration-interaction predictions). The key finding is that the lowest-energy spin excitation, that is, S_A for the (1,0) state and S_C for the (0,2) state, does not shift as we go through the ground-state transition (Fig. 3). As pointed out above, this is precisely the molecular signature in the quantum dot, where the rigid rotation of the electrons is decoupled from the relative-motion dynamics. This experimental result is in sharp contrast with that theoretically expected in the absence of correlation. In fact, the S_A and S_C transitions occur at $\sim\hbar\omega_0$, and therefore are strongly renormalized with respect to the value of $\sim 2\hbar\omega_0$ at which the weak single-particle modes appear in the limit $r_S \to 0$. In addition, with no correlation, the S_A and S_C modes experience a large exchange-energy splitting $J \sim (\hbar\omega_0)^{1/2}$ (see Supplementary Information, Fig. S2, Methods and Discussion), as confirmed by our self-consistent Hartree–Fock calculation[29], which predicts a splitting of $\sim$1.5 meV for $r_S = 1.71$ (red vertical lines in the left part of Fig. 3).

The low-lying charge mode for the (1,0) state (C_A in Fig. 3) is replaced for the (0,2) state by a charge excitation (C_B) shifted at slightly higher energy whereas a replica of the spin mode S_C appears in the charge channel owing to the breakdown of the polarization selection rule induced by B (see Supplementary Information, Methods and Discussion and Fig. S1). As for spin excitations (Fig. 2a), the energies of charge excitations agree with those predicted by configuration interaction (Fig. 3, right) whereas the positions of C_A, C_B and S_B peaks are also in contrast with the Hartree–Fock calculations (not shown). The shortcomings of Hartree–Fock point towards interpreting the marginal energy shifts observed for the modes between the two ground states as a manifestation of strong correlation effects leading to the roto-vibrational structure of energy levels. Remarkably, as we argue below, this molecular signature occurs at r_S values for which localization in space of electron wavefunctions is not yet fully achieved.

To gain insight into the relative motion of the electrons for the states experimentally accessed, we use configuration interaction

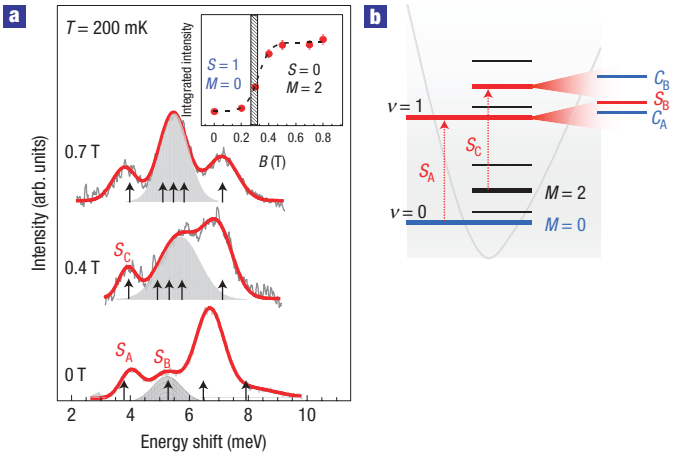

Figure 2 Magnetic-field dependence in quantum dots with four electrons. **a**, Experimental light scattering spectra of monopole spin excitations for three values of B. The red lines are fits to experimental data (grey lines) using three gaussians (four at $B = 0$ T). The shaded areas correspond to a specific gaussian. The arrows indicate the calculated excitations. The inset shows the integrated intensity of the central peak (shaded area) versus B (error bars correspond to standard deviation of the fits). The shaded box indicates the predicted position of the ground-state transition. **b**, A scheme of the roto-vibrational structure in the quantum-dot potential. Transitions S_A and S_C occur between different rotational states belonging to $\nu = 0$ and $\nu = 1$ vibrational levels (see Supplementary Information, Methods and Discussion).

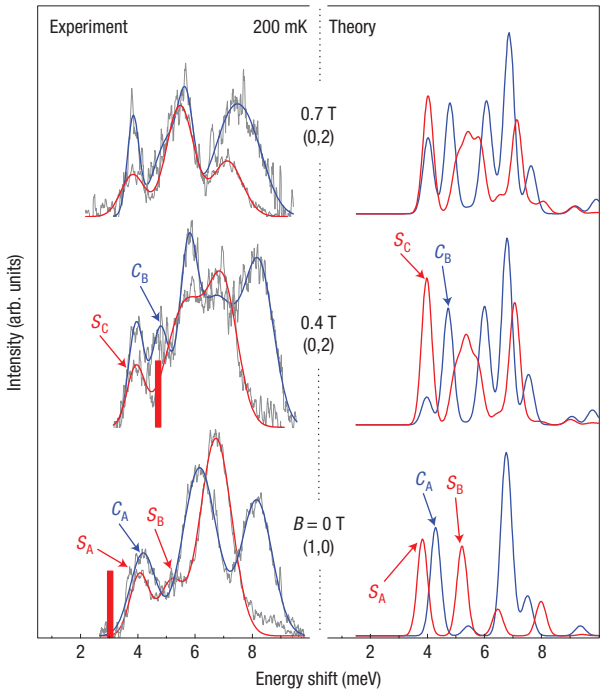

Figure 3 Experimental/theoretical spectra with magnetic fields. Experimental (left column) and computed (right column) spectra for charge (blue lines) and spin (red lines) excitations. The values (S, M) for the ground states are indicated. Blue and red lines in the left column are fits to the experimental data (grey lines) using gaussians. The calculated peaks are artificially broadened using gaussians with standard deviation 0.18 meV, and the laser energy used in the calculation, determined from the optical gap, is $\hbar\omega_L = 6(18)$ meV for charge (spin) excitations (see Supplementary Information, Methods, Discussion and Fig. S1). Vertical red lines in the left panel are the Hartree–Fock predictions for S_A and S_C.

to evaluate the pair correlation function $g(r)$ for the two ground states at theoretically extrapolated densities (Fig. 4a). The quantity $g(r)$—the probability that two electrons are at distance r (see the Methods section)—clearly shows that the internal motion of the electrons depends on M when correlation is negligible ($r_s = 0.1$, Fig. 4a), whereas it is substantially independent already at the experimental density of $r_s = 1.71$. At very small densities ($r_s = 20$, Fig. 4a), the two $g(r)$ values overlap completely and the molecule is a rigid rotor. This crossover is quantitatively studied by computing the functional distance separating $g(r)$ values of pairs of states, $\int_0^\infty dr|g_X(r) - g_{X'}(r)|r$, where X (X') is a state depending on $M = 0$ ($M = 2$). This is shown in Fig. 4b for the ground states (black curve) and the two lowest-energy spin excitations S_A, S_C (red curve). The change in the slope of the functional distance, very close to the experimental value of r_s (the vertical bar in Fig. 4b), points to a transition from a liquid-like state at small r_s to a molecule at large r_s. Remarkably, the critical value of r_s is the same for both ground states and spin excitations.

The discovered transition to this correlated state is distinct from Wigner spatial localization of electrons, which emerges at larger values of r_s in the intrinsic reference frame of the molecule. Wigner localization is seen by fixing the position of one electron in the xy plane (filled black circles in Fig. 4d), and then evaluating the conditional probability of measuring another electron[3] (see the Methods section). This conditional probability is plotted as contour plots in Fig. 4d for the $M = 2$ ground state (left column) and the S_C excited state (right column), respectively, for increasing values of r_s (from top to bottom). Whereas in the non-interacting case ($r_s = 0.1$) the only structure is the exchange hole around the fixed electron, at the experimental value of r_s (centre panels of Fig. 4d) weight is moved away from the latter owing to correlation. As r_s is increased (bottom panels of Fig. 4d), electrons localize at the vertices of a square in the $M = 2$ ground state, whereas the charge distribution of S_C is consistent with the lowest-energy B_1 normal mode of vibration for the C_{4v} point symmetry group of the square (white diagrams in Fig. 4d and Supplementary Information, Methods and Discussion).

To assess the threshold for Wigner localization, we also compute the spin-resolved probability density $n_\sigma(r)$ of the triplet ground state with spin projection $S_z = 1$, and evaluate the functional distance between $n_+(r)$ and $n_-(r)$, $\int_0^\infty dr|n_+(r) - n_-(r)|r$, plotted in Fig. 4c (see the Methods section). As there are three spin-up electrons and one spin-down electron, the difference is expected to vanish only in the limit $r_s \to \infty$, when the overlap among the wavefunctions of fully localized electrons becomes negligible as well as their mutual exchange interaction, making the spin degree of freedom irrelevant. In contrast with Fig. 4b, the variation of the slope of the curve in Fig. 4c is smooth with r_s, showing that no sharp boundary for electron localization can be found[14]. Exchange interaction between partially localized electrons also explains the fine structure of roto-vibrational levels highlighted in the energy scheme in Fig. 2b. We have checked that for large values of r_s the energy splitting between the excitations S_A, S_B, S_C and C_B becomes negligible and all of the states collapse into the same B_1 roto-vibrational band (see Supplementary Information, Methods, Discussion and Table S2).

METHODS

EXPERIMENTAL SET-UP

The sample was placed in a dilution magnetocryostat reaching temperatures under illumination down to 200 mK. A tunable Ti:sapphire continuous-wave

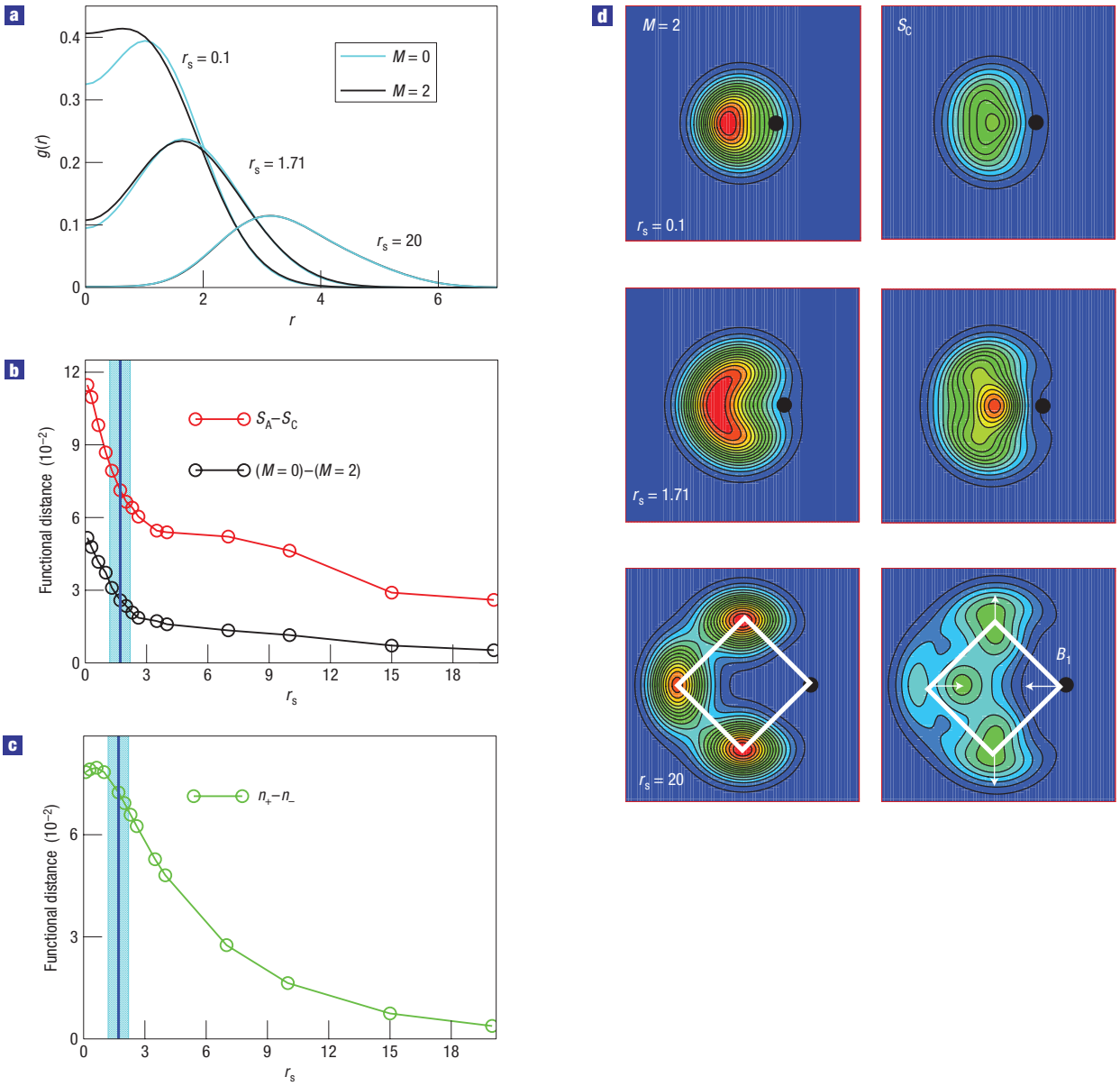

Figure 4 Theoretical analysis of molecule formation extrapolated to the full density range. The unit length is $(\hbar/m^*\omega_0)^{1/2}$. **a**, $g(r)$ versus r for the two ground states. **b**, Distance $\int_0^\infty \mathrm{d}r|g_X(r)-g_{X'}(r)|r$ versus r_s for two pairs of states (X, X'), where the first (second) pair consists of the two ground states (S_A and S_C). The vertical bar width is obtained from the B range of the ground-state transition. **c**, Distance between $n_+(r)$ and $n_-(r)$ versus r_s, for the triplet ground state with $S_z = 1$. **d**, Probability of measuring an electron in the xy plane provided another one is fixed at position $(x, y) = (x_0, 0)$ labelled by a black dot, where x_0 is located at the average value of r. The squares' size is 8×8, and the 15 equally spaced contour levels go from blue (minimum) to red (maximum). The normalization is the same within each row.

single-mode laser with frequency ω_L (close to 1,560 meV) was used as the excitation source. The scattered light from the quantum-dot array at ω_S was collected through a series of optics, dispersed by a triple-grating spectrometer and detected by a CCD (charge-coupled device) camera (Fig. 1a). Samples were fabricated from a 25-nm-wide, one-side modulation-doped $Al_{0.1}Ga_{0.9}As/GaAs$ quantum well (density $n = 1.1 \times 10^{11}$ cm^{-2} and mobility $\mu \approx 3 \times 10^6$ cm^2 V^{-1} s^{-1}) by electron beam lithography and inductively coupled plasma reactive ion etching.

INELASTIC LIGHT SCATTERING

Neutral electronic excitations in GaAs quantum dots can be classified in terms of changes of total angular momentum ΔM and total spin ($\Delta S = 0$ for charge excitations, $\Delta S = \pm 1$ for spin excitations) and can be selectively probed by setting the linear polarizations (parallel for charge and perpendicular for spin) of the incident and scattered photons, respectively[17–19]. The parity selection rule dictates that monopole excitations with $\Delta M = 0$ are the strongest modes active in the inelastic light scattering experiments in the backscattering configuration. Partial breakdown of the polarization selection rule occurs in our quantum dots at finite values of an applied magnetic field (see Supplementary Information, Methods and Discussion). By comparing spin and charge spectra, direct evaluation of the impact of few-body effects may be inferred by measuring their energy position and splitting[19].

EVIDENCE FOR THE FOUR-ELECTRON QUANTUM-DOT POPULATION

To achieve the four-electron population, different quantum-dot arrays with D between 240 and 180 nm were nanofabricated. Identification of this number

of electrons is linked to the observation of the spin mode labelled S_B (Fig. 2). The assignment of the S_B mode is confirmed by the theoretical evaluations based on a full configuration-interaction calculation[20] (the Raman-active configuration-interaction excitations labelled by the arrows in Fig. 2a). Contrary to the other spin peaks seen in the spectrum of Fig. 2a at $B = 0$ T, the S_B mode is not observed in other quantum dots with different D. The rapid disappearance of the S_B mode above 2 K (not shown), owing to the thermal occupation of a low-lying singlet state, independently confirms the nature of this peak[19].

CALCULATION OF THE ENERGY SPECTRUM AND WAVEFUNCTIONS

We used the full configuration-interaction approach[20] to solve with high numerical accuracy the few-body problem of N interacting electrons associated with the hamiltonian:

$$H = \sum_{i=1}^{N} (\mathbf{p}_i - e\mathbf{A}(\mathbf{r}_i)/c)^2/2m^* + m^*\omega_0^2(x_i^2+y_i^2)/2 + V(z_i) + g_e\mu_B B s_{iz} + \sum_{i<j} e^2/\kappa_r|\mathbf{r}_i - \mathbf{r}_j|.$$

Here, the conduction band electrons are trapped in a dot confined in the xy plane by a harmonic potential with interlevel energy spacing $\hbar\omega_0 = 3.75$ meV as well as along z by the potential $V(z)$ of a symmetric square quantum well (whose width is 25 nm and energy offset 250 meV). $\mathbf{r}_i \equiv (x_i, y_i, z_i)$ is the position of the ith electron, $\mathbf{p}_i$ its canonically conjugated momentum, $\mathbf{A}(\mathbf{r}) = B\hat{\mathbf{z}} \times \mathbf{r}/2$ is the vector potential giving rise to the magnetic field B along z, $m^* = 0.067m_e$ is the GaAs conduction band effective mass, m_e and e are the free electron mass and charge, respectively, $g_e = -0.44$ is the bulk GaAs gyromagnetic factor, μ_B is the Bohr magneton, s_{iz} is the z component of the spin of the ith particle, $\kappa_r = 12.4$ is the relative dielectric constant and c is the speed of light. The eigenstates of H are superpositions of Slater determinants, $\prod_{i=1}^{N} \hat{c}_{\alpha_i}^{+}|0\rangle$, which are obtained by filling in the single-particle spin–orbitals α with the N electrons in all possible ways, where the second-quantization operator $\hat{c}_\alpha^+$ creates an electron in level $\alpha \equiv (n, m, s_z)$ when applied to the vacuum, $|0\rangle$. Here, n and m are the radial and azimuthal quantum numbers of Fock–Darwin orbitals[1], respectively, which we included up to the 10th energy shell. Such orbitals, multiplied by the ground state of the well $V(z)$, are the eigenstates of the non-interacting part of H. The whole interacting hamiltonian H, a matrix with respect to the basis of the Slater determinants, is first block diagonalized, where the blocks are labelled by the total orbital angular momentum, M, total spin, S, and its z projection, S_z (the symmetry-breaking effect of the Zeeman term is neglected here). Finally, each block is diagonalized using the Lanczos method[20], yielding both eigenvalues and eigenstates at low energy (the block maximum linear size was 5.1×10^4). The accuracy of the calculation was estimated by comparing the analytically known value of the dipole Kohn excitation mode, $\hbar\omega_0$ at $B = 0$ T, with that calculated using full configuration interaction. The relative error for excitation energies, in the worst case of $r_s = 22$, was less than 7×10^{-3}.

CALCULATION OF DENSITY AND CORRELATION FUNCTIONS

The spin-resolved probability density $n_\sigma(r)$, where $\sigma = +, -$ and $r = \sqrt{x^2+y^2}$, is computed as the quantum average over a given configuration-interaction state, $n_\sigma(r) = (1/N_\sigma)\int dz \langle \sum_{i=1}^{N} \delta(\mathbf{r} - \mathbf{r}_i)\delta_{\sigma,\sigma_i}\rangle$, where N_σ is the number of electrons with spin σ. The total density is $n(r) = [N_+ n_+(r) + N_- n_-(r)]/N$. The conditional probability plotted in Fig. 4d is defined as $P(x, y; x_0, y_0) = (1/N(N-1))\langle \sum_{i,j=1}^{N} \delta(\mathbf{r} - \mathbf{r}_i)\delta(\mathbf{r}_0 - \mathbf{r}_j)\rangle$, where (x_0, y_0) is fixed at the average value of r and z, z_0 are fixed at the centre of the quantum well. The correlation function $g(r)$ is obtained by integration of P over the centre-of-mass coordinate, $g(r) = A\int P(x/2 + X, y/2 + Y; -x/2 + X, -y/2 + Y)dXdY$, where the prefactor A is chosen so that $\int_0^\infty dr g(r) r = 1$.

Received 15 January 2008; accepted 18 March 2008; published 20 April 2008.

References

1. Jacak, L., Hawrylak, P. & Wójs, A. *Quantum Dots* (Springer, Berlin, 1998).
2. Chakraborty, T. *Quantum Dots—A Survey of the Properties of Artificial Atoms* (North-Holland, Amsterdam, 1999).
3. Reimann, S. M. & Manninen, M. Electronic structure of quantum dots. *Rev. Mod. Phys.* **74**, 1283–1342 (2002).
4. Bryant, G. W. Electronic structure of ultrasmall quantum-well boxes. *Phys. Rev. Lett.* **59**, 1140–1143 (1987).
5. Maksym, P. A. & Chakraborty, T. Quantum dots in a magnetic field: Role of electron–electron interactions. *Phys. Rev. Lett.* **65**, 108–111 (1990).
6. Häusler, W. & Kramer, B. Interacting electrons in a one-dimensional quantum dot. *Phys. Rev. B* **47**, 16353–16357 (1993).
7. Eric Yang, S.-R., MacDonald, A. H. & Johnson, M. D. Addition spectra of quantum dots in strong magnetic field. *Phys. Rev. Lett.* **71**, 3194–3197 (1993).
8. Egger, R., Häusler, W., Mak, C. H. & Grabert, H. Crossover from Fermi liquid to Wigner molecule behavior in quantum dots. *Phys. Rev. Lett.* **82**, 3320–3323 (1999).
9. Yannouleas, C. & Landman, U. Electron and boson clusters in confined geometries: Symmetry breaking in quantum dots and harmonic traps. *Proc. Natl Acad. Sci. USA* **103**, 10600–10605 (2006).
10. Maksym, P. A., Imamura, H., Mallon, G. P. & Aoki, H. Molecular aspects of electron correlation in quantum dots. *J. Phys. Condens. Matter* **12**, R299–R334 (2000).
11. Filinov, A. V., Bonitz, M. & Lozovik, Y. E. Wigner crystallization in mesoscopic 2D electron systems. *Phys. Rev. Lett.* **86**, 3851–3854 (2001).
12. Koskinen, M., Manninen, M., Mottelson, B. & Reimann, S. M. Rotational and vibrational spectra of quantum rings. *Phys. Rev. B* **63**, 205323 (2001).
13. Rontani, M., Goldoni, G., Manghi, F. & Molinari, E. Raman signatures of classical and quantum phases in coupled dots: A theoretical prediction. *Europhys. Lett.* **58**, 555–561 (2002).
14. Ghosal, A., Güçlü, A. D., Umrigar, C. J., Ullmo, D. & Baranger, H. U. Correlation-induced inhomogeneity in circular quantum dots. *Nature Phys.* **2**, 336–340 (2006).
15. Landau, L. D. & Lifshitz, E. M. *Quantum Mechanics: Non-Relativistic Theory* (Pergamon, Oxford, 1977).
16. Strenz, R. *et al.* Single-particle excitations in quasi-zero- and quasi-one-dimensional electron systems. *Phys. Rev. Lett.* **73**, 3022–3025 (1994).
17. Lockwood, D. J. *et al.* Shell structure and electronic excitations of quantum dots in a magnetic field probed by inelastic light scattering. *Phys. Rev. Lett.* **77**, 354–357 (1996).
18. Schüller, C. *et al.* Quasiatomic fine structure and selection rules in quantum dots. *Phys. Rev. Lett.* **80**, 2673–2676 (1998).
19. García, C. P. *et al.* Evidence of correlation in spin excitations of few-electron quantum dots. *Phys. Rev. Lett.* **95**, 266806 (2005).
20. Rontani, M., Cavazzoni, C., Bellucci, D. & Goldoni, G. Full configuration interaction approach to the few-electron problem in artificial atoms. *J. Chem. Phys.* **124**, 124102 (2006).
21. Leggett, A. J. *Quantum Liquids* (Oxford Univ. Press, Oxford, 2006).
22. Kalliakos, S. *et al.* Photoluminescence of individual doped GaAs/AlGaAs nanofabricated quantum dots. *Appl. Phys. Lett.* **90**, 181902 (2007).
23. Kalliakos, S. *et al.* Optical control of energy-level structure of few electrons in AlGaAs/GaAs quantum dots. *Nano Lett.* **8**, 577–581 (2008).
24. Kouwenhoven, L. P. *et al.* Excitation spectra of circular, few-electron quantum dots. *Science* **278**, 1788–1792 (1997).
25. Heitmann, D. & Kotthaus, J. P. The spectroscopy of quantum dot arrays. *Phys. Today* **46**, 56–63 (1993).
26. Ellenberger, C. *et al.* Excitation spectrum of two correlated electrons in a lateral quantum dot with negligible Zeeman splitting. *Phys. Rev. Lett.* **96**, 126806 (2006).
27. Nishi, Y. *et al.* Intermediate low spin states in a few-electron quantum dot in the $\nu \leq 1$ regime. *Phys. Rev. B* **74**, 033306 (2006).
28. Jiang, H. W. *et al.* Quantum liquid versus electron solid around $\nu = 1/5$ Landau-level filling. *Phys. Rev. Lett.* **65**, 633–636 (1990).
29. Rontani, M., Rossi, F., Manghi, F. & Molinari, E. Coulomb correlation effects in semiconductor quantum dots: The role of dimensionality. *Phys. Rev. B* **59**, 10165–10175 (1999).

Supplementary Information accompanies this paper on www.nature.com/naturephysics.

Acknowledgements

This work was supported by the projects MIUR-FIRB No. RBIN04EY74 and No. RBIN06JB4C, PRIN 2006 No. 2006022932 'Few-electron phenomena in semiconductor-quantum-dot devices', and the INFM-CINECA Supercomputing Project 2007. A.P. is supported by the National Science Foundation under Grant No. DMR-0352738, by the Department of Energy under Grant No. DE-AIO2-04ER46133, and by a research grant from the W. M. Keck Foundation. We thank F. Beltram, S. Corni and R. Fazio for useful discussions.

Author contributions

The nanofabrication and experiments were carried out by S.K., V.P., C.P.G. and A.P.; M.R., G.G. and E.M. were responsible for the theoretical analysis; L.N.P. and K.W.W. provided the modulation-doped quantum-well samples.

Author information

Reprints and permission information is available online at http://npg.nature.com/reprintsandpermissions. Correspondence and requests for materials should be addressed to M.R. or V.P.